

# RNG: Relightable Neural Gaussians

JIAHUI FAN, Nanjing University of Science and Technology, China

FUJUN LUAN, Adobe Research, USA

JIAN YANG<sup>†</sup>, Nanjing University of Science and Technology, China

MILOŠ HAŠAN, Adobe Research, USA

BEIBEI WANG<sup>†</sup>, Nanjing University, China



Fig. 1. We propose *RNG: Relightable Neural Gaussians*, achieving high-quality relighting under novel views with sharp details. With the implicit neural representation of materials, we avoid any assumptions of geometry types, enabling relighting for both hard surfaces and fluffy shapes. Our method achieves highly efficient training (within 1.5 hours) and rendering (60 fps) on an RTX4090 GPU.

3D Gaussian Splatting (3DGS) has shown its impressive power in novel view synthesis. However, creating relightable 3D assets, especially for objects with ill-defined shapes (e.g., fur), is still a challenging task. For these scenes, the decomposition between the light, geometry, and material is more ambiguous, as neither the surface constraints nor the analytical shading model hold. To address this issue, we propose RNG, a novel representation of *relightable neural Gaussians*, enabling the relighting of objects with both hard surfaces or fluffy boundaries. We avoid any assumptions in the shading model but maintain feature vectors, which can be further decoded by an MLP into colors, in each Gaussian point. Following prior work, we utilize a point light to reduce the ambiguity and introduce a shadow-aware condition to the network. We additionally propose a depth refinement network to help the shadow computation under the 3DGS framework, leading to better shadow effects under point lights. Furthermore, to avoid the blurriness brought by the alpha-blending in 3DGS, we design a hybrid forward-deferred optimization strategy. As a result, we achieve about 20× faster in training and about 600× faster in rendering than prior work based on neural radiance fields, with 60 frames per second on an RTX4090.

CCS Concepts: • Computing methodologies → Rendering.

<sup>†</sup>Corresponding authors. Email: csjyang@njust.edu.cn, beibei.wang@nju.edu.cn.  
Authors' addresses: Jiahui Fan, Nanjing University of Science and Technology, China, fjh@njust.edu.cn; Fujun Luan, Adobe Research, USA, fluan@adobe.com; Jian Yang<sup>†</sup>, Nanjing University of Science and Technology, China, csjyang@njust.edu.cn; Miloš Hašan, Adobe Research, USA, milos.hasan@gmail.com; Beibei Wang<sup>†</sup>, Nanjing University, China, beibei.wang@nju.edu.cn.

Permission to make digital or hard copies of all or part of this work for personal or classroom use is granted without fee provided that copies are not made or distributed for profit or commercial advantage and that copies bear this notice and the full citation on the first page. Copyrights for components of this work owned by others than ACM must be honored. Abstracting with credit is permitted. To copy otherwise, or republish, to post on servers or to redistribute to lists, requires prior specific permission and/or a fee. Request permissions from permissions@acm.org.

© 2024 Association for Computing Machinery.

0730-0301/2024/10-ART \$15.00

<https://doi.org/10.1145/nnnnnnnn.nnnnnnn>

Additional Key Words and Phrases: neural rendering, Gaussian splatting, relighting

## ACM Reference Format:

Jiahui Fan, Fujun Luan, Jian Yang<sup>†</sup>, Miloš Hašan, and Beibei Wang<sup>†</sup>. 2024. RNG: Relightable Neural Gaussians. *ACM Trans. Graph.* 1, 1 (October 2024), 10 pages. <https://doi.org/10.1145/nnnnnnnn.nnnnnnn>

## 1 INTRODUCTION

Creating relightable 3D assets from multi-view images captured in the real world is an effective way for 3D content creation, avoiding tedious manual labor. Unfortunately, this task is still challenging because of the ill-posed nature of the decomposition between lighting, materials, and geometries. In particular, the created 3D asset could be an object with well-defined surfaces or ill-defined shapes (e.g., fur, grass, etc.), as both are important in many applications. Unfortunately, this generalization requirement raises difficulties in decomposition, as no surface-specific constraint or analytical shading models can be leveraged. In this paper, we aim to relight objects with both clear surfaces and fluffy shapes given multi-view images, simultaneously achieving high-quality relighting and shortening training/rendering time costs.

Extensive efforts have been made to reconstruct relightable 3D assets by using the neural radiance field (NeRF) [Mildenhall et al. 2021] or 3D Gaussian splatting (3DGS) [Kerbl et al. 2023]. Most of the existing approaches based on NeRF [Jin et al. 2023; Li et al. 2024; Liu et al. 2023; Wang et al. 2021] or 3DGS [Gao et al. 2023; Jiang et al. 2024; Liang et al. 2024] introduce surface constraints to reduce the ambiguities between geometry and materials. However, they rely on surface shading models, preventing them from reconstructing fluffy objects. The other line of work enables the relighting of clear surfaces and fluffy objects via neural shading models [Zeng et al.

2023]. While their method can achieve high quality, it suffers from over-smooth shapes and numerous training/rendering time costs.

In this paper, we propose *Relightable Neural Gaussians* (RNG), a novel framework for relighting objects with both clear surfaces and fluffy shapes. Instead of trying to explicitly decompose the light and materials, we propose to implicitly model a *relightable radiance representation* from surfaces or volumes of the object, so that the assumptions in shading models can be avoided. We leverage an implicit way by conditioning the light directions into a neural representation of the colors from each Gaussian, making the radiance representation relightable. This way, both the direct and indirect lighting can be modeled at the same time. Following Zeng et al. [2023], we utilize a moving point light to reduce the ambiguities in decomposition.

Shadows from a point light source are sharp, which makes it challenging for the neural network to represent. Therefore, we present a shadow-aware conditioning with depth refinement for the relightable radiance representation, via an adopted shadow mapping. By modeling the visibility between the point light and the shading points, we achieve better-characterized shadows. Also, the shadows tend to be blurry due to the alpha blending of the visibility. Although applying deferred shading can partially solve this issue, it brings obvious outliers and severe floaters issue to the geometry. Based on these observations, we introduce a hybrid optimization pipeline, starting with forward shading and followed by deferred shading for better shadow appearance.

Consequently, RNG achieves high quality in relighting under point light conditions, and shows more detailed results for fluffy objects, compared to NeRF-based prior work [Zeng et al. 2023]. In terms of performance, RNG is about 20× faster in training and about 600× faster than Zeng et al. [2023] in rendering, achieving a 60 frame rate on an RTX4090.

To summarize, our main contributions include

- RNG, the relightable neural Gaussians, using neural implicit relightable radiance representation, enabling relighting of both clear surfaces and fluffy shapes at a low cost of training and rendering time,
- a shadow-aware condition with depth refinement for the relightable radiance field, enhancing the quality of shadows, and
- a hybrid (forward-deferred) optimization strategy, achieving high-quality geometry and sharp shadows.

## 2 RELATED WORK

### 2.1 Neural implicit scene representations

NeRF [Mildenhall et al. 2021] provides a general solution for novel view synthesis (NVS). Since then, numerous work [Barron et al. 2022; Chen et al. 2022; Fridovich-Keil et al. 2022; Müller et al. 2022] have been proposed and significantly pushed the progress of 3D vision. NeRF-based methods obtain a neural implicit representation with Multi-layer Perceptrons (MLPs) [Barron et al. 2021, 2022; Verbin et al. 2022], and differentiable volume rendering is utilized in the optimization. Sometimes, to reconstruct high-quality surfaces or meshes, signed distance functions (SDFs) are also widely linked into the representations [Rosu and Behnke 2023; Wang et al. 2021, 2023],

leading to smoother surface normals but even slower rendering. Some use grid-like representations [Chen et al. 2022; Fridovich-Keil et al. 2022; Müller et al. 2022] to accelerate the training and rendering, while also providing reliable geometric priors.

3DGS [Kerbl et al. 2023] brings the rasterization framework into multi-view stereo reconstructions. In contrast to NeRF-based methods, 3DGS doesn't represent the scenes in a volumetric way but adopts discrete 3D Gaussian primitives for scene representation. Objects are represented by 3D Gaussians and are splatted onto the image plane with alpha-blended colors, leading to impressive NVS quality and remarkable real-time performance. However, this nature of 3DGS also hurts the quality of its obtained depth and normal, making them noisy and difficult for further use. Some existing methods [Dai et al. 2024; Guédon and Lepetit 2024; Huang et al. 2024] bring constraints or build meshes from the Gaussians, significantly improve the geometry quality. Particularly, Chen et al. [2023] combine NeuS and 3DGS together and jointly optimize them, significantly improving the surface reconstruction quality.

Compared to NeRF-based methods, 3DGS-based methods are more efficient, and enjoy the flexible distributions of Gaussian points, representing fluffy objects better. Adding geometric priors (e.g., surface assumptions) can significantly improve the NVS quality for objects with hard surfaces, but fails with fluffy shapes. Therefore, we choose to use 3DGS as the basic framework without introducing any surface priors. Some extra components can also be introduced to our framework to further refine the NVS quality, which is orthogonal to our work. We leave this for future work.

### 2.2 Inverse rendering

Given multi-view RGB images, inverse rendering can decompose the geometry, material, and light, and these assets can be reused under any desired novel lighting. To represent the materials, most methods introduce the Disney Principled BRDF model [Burley and Studios 2012] as a physically-based prior, and neural materials [Zhang et al. 2021b] is also utilized for material recovery. By modeling the light implicitly or explicitly, NeRF-based methods [Boss et al. 2021a,b; Jin et al. 2023; Yang et al. 2023; Zhang et al. 2023b, 2021a] produces high-quality inverse rendering at the cost of high training consumption and slow rendering speed. Zhang et al. [2023a] adopts the SGGX Microflake model [Heitz et al. 2015] to perform inverse rendering, achieving unique effects for semi-transparent and fluffy targets.

Recently, 3DGS-based methods have drawn attention in the field of inverse rendering by applying multiple regularizations to Gaussians. Jiang et al. [2024] and Shi et al. [2023] propose to combine the axes of Gaussians with the normals of the objects. Gao et al. [2023] and Liang et al. [2024] also use the normal obtained from depth as supervision. Liu et al. [2023] propose two light representations to help the relighting of objects.

Decomposing materials, geometries, and light explicitly usually requires a fixed type of analytical model. Such assumptions are powerful in reducing ambiguity, but inflexible in including various types of objects. Almost none of these methods can handle the relighting of fluffy objects. In contrast, our method doesn't rely on such assumptions. Additionally, having explicit light transport models means extra computational overhead for global illumination,

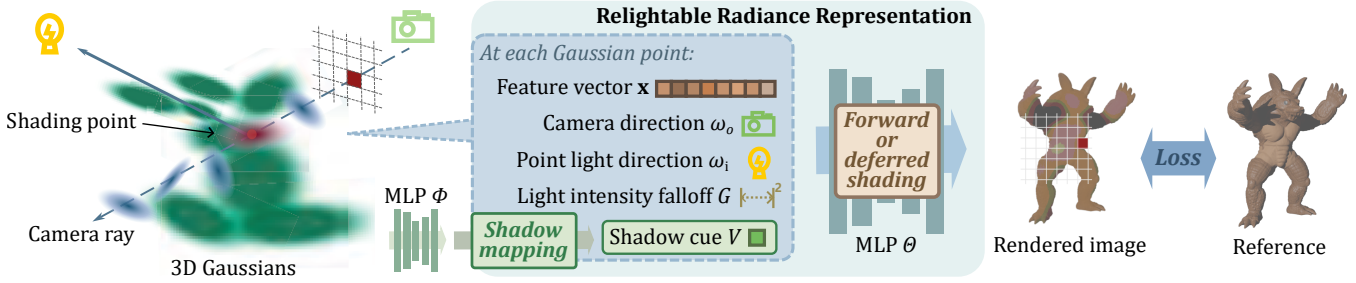


Fig. 2. The overview of RNG pipeline. We propose the relightable radiance representation to achieve relighting for both surface-based and fluffy objects without any assumptions. We use latent vectors  $x$  in each Gaussian point to describe the appearance attributes, and decode them with view/light directions ( $\omega_i, \omega_o$ ) to achieve the relightability. We propose a shadow-aware condition  $V$  (the shadow cue) via an adopted shadow mapping process to condition the decoder MLP  $\Theta$ . In order to improve the quality of shadow regions, we deploy a depth refinement MLP  $\Phi$  before casting the shadow mapping, as well as a hybrid forward-deferred optimization strategy. We describe the details of the shadow-aware conditioning in Sec. 3.3 and the hybrid optimization in Sec. 3.4, respectively.

while the radiance representation can naturally include indirect lighting. Therefore, we propose neural implicit relightable radiance representation for the ease of a wider range of scenarios.

### 2.3 Relighting of ill-defined shapes

Image-based relighting has been widely researched in past years. Some early approaches propose to use neural interpolation [Bemana et al. 2020], introduce physically-based light transport prior [Ren et al. 2015], or pretrain a model on public datasets [Xu et al. 2018]. However, all these methods cannot simply extend to fluffy objects, due to the complex light transport approximation or the absence of such datasets. Later, Gao et al. [2020] present Deferred Neural Relighting, which leverages learned neural texture on a rough proxy geometry for relighting objects including fluffy shapes with a neural renderer. Recently, Zeng et al. [2023] propose NRHnts, which maintains an implicit neural representation with both SDF and NeRF-style feature grids, and predicts radiance with shadow and highlight hints, achieving relighting for both surface objects and fluffy objects with high quality. Mullia et al. [2024] propose a novel representation that combines explicit geometry with a neural feature grid and an MLP decoder, achieving high-fidelity rendering and relighting with good flexibility and integration.

In terms of capability and applications, NRHnts is the most closed approach to our work. Since we leverage the 3DGS framework and don't introduce any surface constraints, RNG enjoys higher training and rendering performance and can avoid the over-smoothed issue.

## 3 METHOD

The goal of our work is to reconstruct high-quality relightable assets for objects with both hard surfaces and fluffy shapes while maintaining short training and rendering time. The core challenge stems from the diverse collection of objects, including both surface-like and fluffy objects. With this subject, neither the assumptions on the geometry regularization nor the surface shading model hold. Therefore, we propose the relightable radiance representation (Sec. 3.2) to implicitly model the light transports, and opt for 3DGS as our

underlying framework due to its high efficiency in training and rendering. Apart from these, we also apply a shadow-aware condition with depth refinement (Sec. 3.3) to the representation to improve the quality of shadows and design a hybrid optimization strategy (Sec. 3.4) to further improve the shadow quality while preserving the quality of geometry. Fig. 2 shows the overall pipeline of our method.

### 3.1 Background: 3DGS and radiance representation

3DGS represents a scene with a set of 3D Gaussians whose distribution is defined as

$$G(x) = e^{-\frac{1}{2}(x-\mu)^T \Sigma^{-1}(x-\mu)}, \quad (1)$$

where  $x$  is a position in the scene,  $\mu$  is the mean of the Gaussian, and  $\Sigma$  denotes the covariance matrix of the 3D Gaussian, which is factorized into a scaling matrix  $S$  and a rotation matrix  $R$  as  $\Sigma = RSS^T R^T$ . To render an image, 3DGS projects the 3D Gaussians onto the image plane and employs alpha blending on the sorted 2D Gaussians as

$$C = \sum_{i \in \mathbb{N}} c_i \alpha_i \prod_{j=1}^{i-1} (1 - \alpha_j), \quad (2)$$

where  $c_i$  is the color of each Gaussian, and  $\alpha_i$  is given by evaluating a projected 2D Gaussian with covariance  $\Sigma'$  multiplied with a learned per-point opacity.

In 3DGS, the alpha-blending of color  $c_i$  from every nearby Gaussian point yields the radiance at position  $x$ . However, given the very naive way that representing the radiance as spherical harmonics, one can alternatively model the radiance at each position in a scene in multiple ways, either explicitly or implicitly.

According to the Rendering Equation [Kajiya 1986], the radiance of a non-emissive object at position  $x$  can be formulated as

$$L_r(x) = \int_{\Omega} F_r(x, \omega_i, \omega_o) L_i(x, \omega_i) \langle \omega_i, n \rangle d\omega_i, \quad (3)$$

where  $F_r$  is the material response at incoming direction  $\omega_i$  and outgoing direction  $\omega_o$ ,  $L_i$  is the light,  $\Omega$  is the upper hemisphere, and  $n$  is the surface normal. In practice, many prior work approximates the rendering equation to get their *explicit* radiance representation,

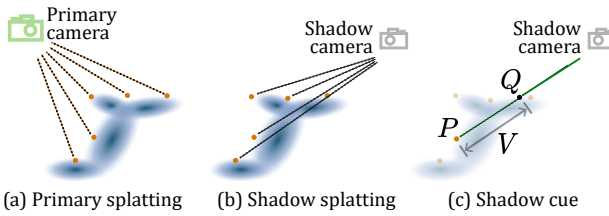


Fig. 3. The formulation of the shadow-aware condition. Inspired by shadow mapping, we obtain the shadow cue in three steps: (a) we first splat all Gaussians onto the primary camera to get the coordinates of the shading point  $P$ . (b) Then we set a shadow camera at the point light location, and splat those Gaussians again to find the shadow ray intersection  $Q$ . (c) After that, a shadow cue  $V$  is computed as the distance between  $P$  and  $Q$  for each pixel to condition the MLP. In practice, we apply a 0-1 clamping operation to improve the stability of training.

and inverse render the scene with such constraints. For example, Jiang et al. [2024] represents the radiance (color) by

$$c_{\omega_o} = c_d + c_s + c_r, \quad (4)$$

where  $c_d$  is the diffuse color,  $c_s$  is the specular light and  $c_r$  is a residual term. Gao et al. [2023] propose to represent the incident light field by

$$L_{\omega_i} = v \cdot L_{\text{global}} + L_{\text{local}}, \quad (5)$$

where  $v$  is the visibility,  $L_{\text{global}}$  and  $L_{\text{local}}$  is a global and a local component, respectively.

### 3.2 Relightable radiance representation

In the context of representing objects with ill-defined shapes (e.g., furry objects), the key is still to model the changes in appearances with various light conditions. However, in this case, neither the choice of the material model  $F$  nor the computation of illumination  $L_i$  is trivial. Instead of trying to explicitly specify these models, we opt for neural *implicit* representations that are more capable and flexible for the radiance representation of such objects.

We use a learned latent space to implicitly represent the radiance in the scene. As shown in Fig 2, the radiance distribution is stored as latent vectors at every point and can be further decoded by an MLP into radiance values. To enable relightability, we make the radiance representation dependent on not only the view directions but also the light conditions. Therefore, the network can decode and predict the radiance values at novel light conditions. The radiance can be represented as

$$L(\mathbf{x}, \omega_o, \omega_i) = \Theta(\mathbf{x}|\omega_o, \omega_i, G), \quad (6)$$

where  $\mathbf{x}$  is the feature vector at each point,  $\Theta$  is an MLP, and  $G$  is the intensity falloff that equals one over the squared distance from shading points to the point light position.

This way, we have a representation that models radiance at each Gaussian point implicitly as a feature vector, and the feature space can be further decoded by a neural network. When applying novel lighting conditions, the network takes the given point light positions

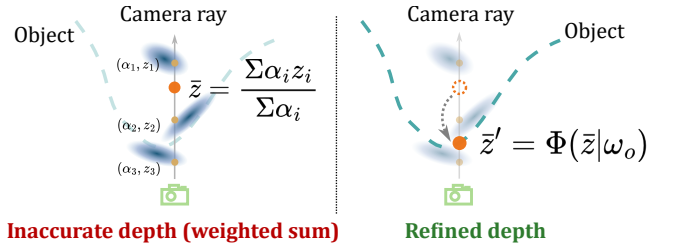


Fig. 4. The effect of the depth refinement network. The weighted sum of Gaussian depths is not accurate. Since the shadow mapping relies on the accurate positioning of all shading points, we propose a depth refinement network to correct the depth from the primary camera. Here we assume the depth error is view-dependent and linear, and use a small MLP  $\Phi$  to predict a scaling factor for each view.

and view directions as conditioning inputs, leading to a neural implicit relightable radiance representation.

### 3.3 Shadow-aware conditioning

With the relightable radiance representation, the radiance at positions in the scene can be represented as latent vectors in each Gaussian point. However, there is a chance that the network overfits all the shadow and light variations under seen light directions, but fails to predict the correct shadow and light with novel point light positions. As a result, the predicted shadow is blurry or incomplete, and be inconsistent across movements. On the other hand, when point lights are introduced, the shape of shadows on the objects is mostly sharp, and the MLP is prone to over-smooth such high-frequency signals. Therefore, it is significant for the network to be aware of the visibility at each shading point.

Inspired by shadow mapping, we introduce a shadow cue to express the visibility information in the scene. However, performing shadow mapping requires the position of all shading points in the scene, while locating the shading points in an implicit scene representation is non-trivial. It usually requires the depth value on camera rays, which is not well-defined for a Gaussian point cloud. Therefore, we also introduce a depth refinement network to help positioning the shading points.

*Depth refinement.* An intuitive and naive proxy for the depth is the weighted sum of the depth and opacity of each Gaussian,

$$\bar{z} = \frac{\sum \alpha_i z_i}{\sum \alpha_i}, \quad (7)$$

where  $z_i$  is the depth value of  $i^{\text{th}}$  Gaussian on the camera ray and  $\alpha_i$  is its opacity. Sometimes the weighted sum is incorrect, leading to wrongly located shading points and consequently mismatching shadow cues. To address this issue, we propose a depth refinement network to correct the shading point locations, as shown in Fig. 4. The refined depth value can be obtained by

$$\bar{z}' = \Phi(\bar{z}|\omega_o), \quad (8)$$

where  $\Phi$  is another MLP. We assume the depth correction is linear for each pixel and dependent on view directions  $\omega_o$ . We run the

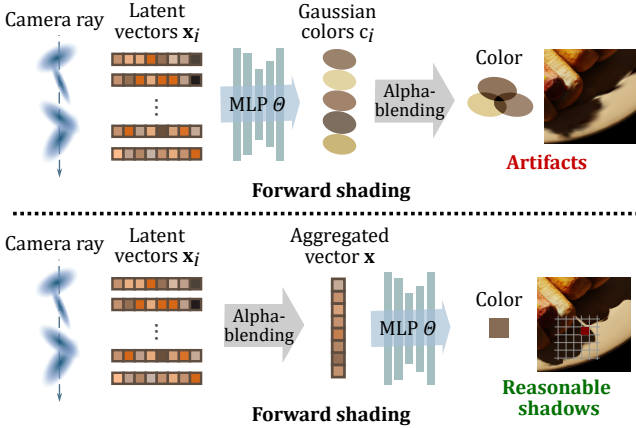


Fig. 5. The difference between forward shading and deferred shading. Through deferred shading, we aggregate all latent vectors along the camera ray according to their opacities and generate a pixel-wise feature vector in the image space for the final decoding. For comparison, the alpha-blending usually leads to wrong and blurry shadows, while deferred shading provides more capability and flexibility to produce plausible colors for the blended image space features.

network before performing the shadow mapping, and it produces better shadows.

*Shadow mapping.* Conventional shadow mapping marches the ray to get visibility, which can be expensive and difficult to achieve. Instead, we perform Gaussian splatting two times to generate a shadow cue map and feed this as a condition into the network. The principle of our adopted shadow mapping is described in Fig. 3. First, we perform Gaussian splatting onto the primary camera to compute the shading points. Then, we set a virtual shadow camera (with the same resolution as the primary camera) at the point light position and rasterize the scene for a second pass to get the intersections of shadow rays and the scene. The distance between shading points and shadow ray intersections is collected as the shadow cue. In the end, the relightable radiance representation has multiple conditions, and all of them contribute to the final color of a single Gaussian point. The final radiance can be represented as

$$L(\mathbf{x}, \omega_o, \omega_i) = \Theta(\mathbf{x} | \omega_o, \omega_i, G, V), \quad (9)$$

where  $V$  is the distance between the Gaussian point and the shadow ray intersection. In practice, we apply a 0-1 clamping to the shadow-aware condition.

With all the formulations above, we now have the RNG framework, where the scene is represented as a structure of Gaussian points, yet the radiance at each Gaussian point is represented as a feature vector that is conditioned on view/light directions and shadow cues. Finally, the adjusted 3DGS rasterization operation appears to be

$$C_{\text{forward}} = \sum_{i \in \mathbb{N}} \Theta(\mathbf{x}_i | \omega_o, \omega_i, G, V) \alpha_i \prod_{j=1}^{i-1} (1 - \alpha_j). \quad (10)$$

### 3.4 Hybrid optimization

Even though the network is aware of visibility information, and the radiance is also conditioned on it, the alpha-blending process after the radiance computation is still harmful to the final shadow quality. The shape of the shadows is produced by blending several Gaussians around the shading point, which leads to blurry and incomplete regions. To address this problem, we suggest a deferred shading process, regularizing the appearance of shadows in the image space. As shown in Fig. 5, the appearance of shadows is not obtained by blending Gaussians, but directly decided in the image space, avoiding the artifacts brought by the blending operation. According to our observation, forward shading produces better geometry, while deferred shading leads to outliers and floaters. Therefore, we design a two-stage optimization strategy to benefit from both options.

*Deferred shading.* In deferred shading, we blend the feature vectors in Gaussian points first to get an aggregated feature in the image space, and then we decode it with the conditional MLP  $\Theta$ , providing view and light directions, and visibility information. In this case, we propose the Gaussian color of deferred RNG as

$$C_{\text{defer}} = \Theta \left( \sum_{i \in \mathbb{N}} \mathbf{x}_i \alpha_i \prod_{j=1}^{i-1} (1 - \alpha_j) | \omega_o, \omega_i, G, V \right). \quad (11)$$

*Two-stage strategy.* We employ the forward RNG in the first stage to get an initial geometry and a latent feature space and turn to deferred shading in the second stage, while re-train the MLP  $\Theta$  from scratch, but keep all the learned latent vectors. Note that in the first stage, we do not enable the shadow cue, since at the early stage the Gaussians are not well-shaped, and the generated wrong shadow information may hurt the training stability.

## 4 IMPLEMENTATION

We implemented our results using Pytorch [Paszke et al. 2019] framework. The feature vectors in each Gaussian are 16-channel, and the MLP is 6-layer with 256 hidden units. We apply frequency encodings to both the view/light directions and the shadow cues, making them 15 dimensions and 17 dimensions, respectively. We use the Adam optimizer [Kingma and Ba 2014] and train it at a learning rate  $1.0 \times 10^{-3}$  for the color decoder MLP,  $3.0 \times 10^{-4}$  for the depth refinement MLP and  $2.5 \times 10^{-3}$  for feature vectors in Gaussian points. We use the same loss functions from Kerbl et al. [2023], which is a combination of  $L_1$  loss and SSIM [Wang et al. 2004].

## 5 RESULTS

In this section, we validate our relighting quality by comparing to NeRF-based prior work (NRHnts) [Zeng et al. 2023] on NRHnts Real/Synthetic [Zeng et al. 2023] and synthetic datasets from RNA [Mullia et al. 2024] to validate the efficiency and effectiveness of our method. All experiments and comparisons are carried out on down-sampled images with  $512 \times 512$  resolution, and with a maximum of 1000 training views used. We run all our results on an RTX4090 GPU and i9-13900K CPU, powered by a Windows Subsystem Linux 2 (Ubuntu 22.04.5) distribution. Note that Zeng et al. [2023] also describe an improved version that uses additional optimization on

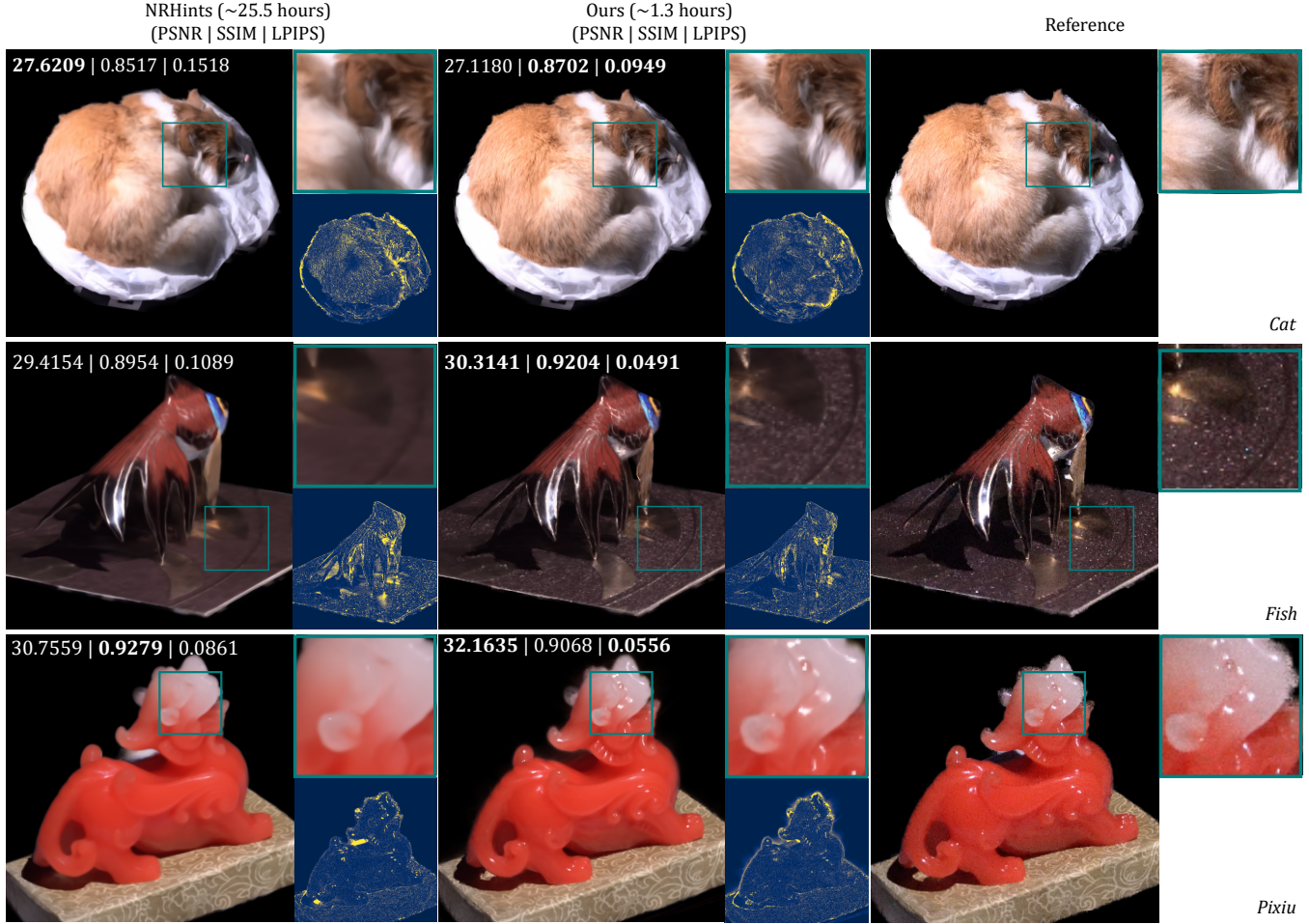


Fig. 6. Comparison between NRHints [Zeng et al. 2023] and our method on real-world objects under point lighting. We provide the peak signal-to-noise ratio (PSNR), structural similarity index (SSIM) [Wang et al. 2004], and learned perceptual image patch similarity (LPIPS) [Zhang et al. 2018] for comparison. Overall, we are about 20x faster in the training speed, and our results have overall lower LPIPS and close PSNR and SSIM values. Our method can produce sharper details and highlights, while the results of NRHints are slightly blurred and over-smoothed in some regions with textures.

camera poses to compensate for the precision of data calibration, but we don't enable it for a fair comparison.

### 5.1 Quality validation

We first validate our relighting quality in both dimensions of visual quality and error statistics across various datasets. Then we show the robustness and consistency of our relighting results under moving lights on both real and synthetic scenes.

In Figs. 6 and 7, we compare our relighting results with NRHints under point lighting on real-world objects and synthetic scenes, respectively. We provide the peak signal-to-noise ratio (PSNR), the structural similarity index (SSIM) [Wang et al. 2004] and learned perceptual image patch similarity (LPIPS) [Zhang et al. 2018] values for comparison, in both dimensions of pixel-wise error and visual reasonableness. In conclusion, our model produces sharper and finer details on hairs and textures with about 20x faster training speed,

compared to the over-smoothed results from NRHints [Zeng et al. 2023].

In Table 1, we report the statistics of our method and NRHints [Zeng et al. 2023] on a series of datasets, including real-world objects and synthetic scenes. Note that our PSNR and SSIM values are close to NRHints [Zeng et al. 2023] and our LPIPS are overall lower, but our training time is less than 1.5 hours, while NRHints [Zeng et al. 2023] takes more than 25 hours to converge.

In Fig. 8, we show the relighting results of RNG under moving lights. Each column in the figure shows a different light direction. Our model can render scenes under novel lights with realistic appearance and high-quality details, and can properly model the self-shadowing effects. The robustness and consistency of our results are also shown by the moving light source. We suggest the reader refer to the supplementary video for more validation.

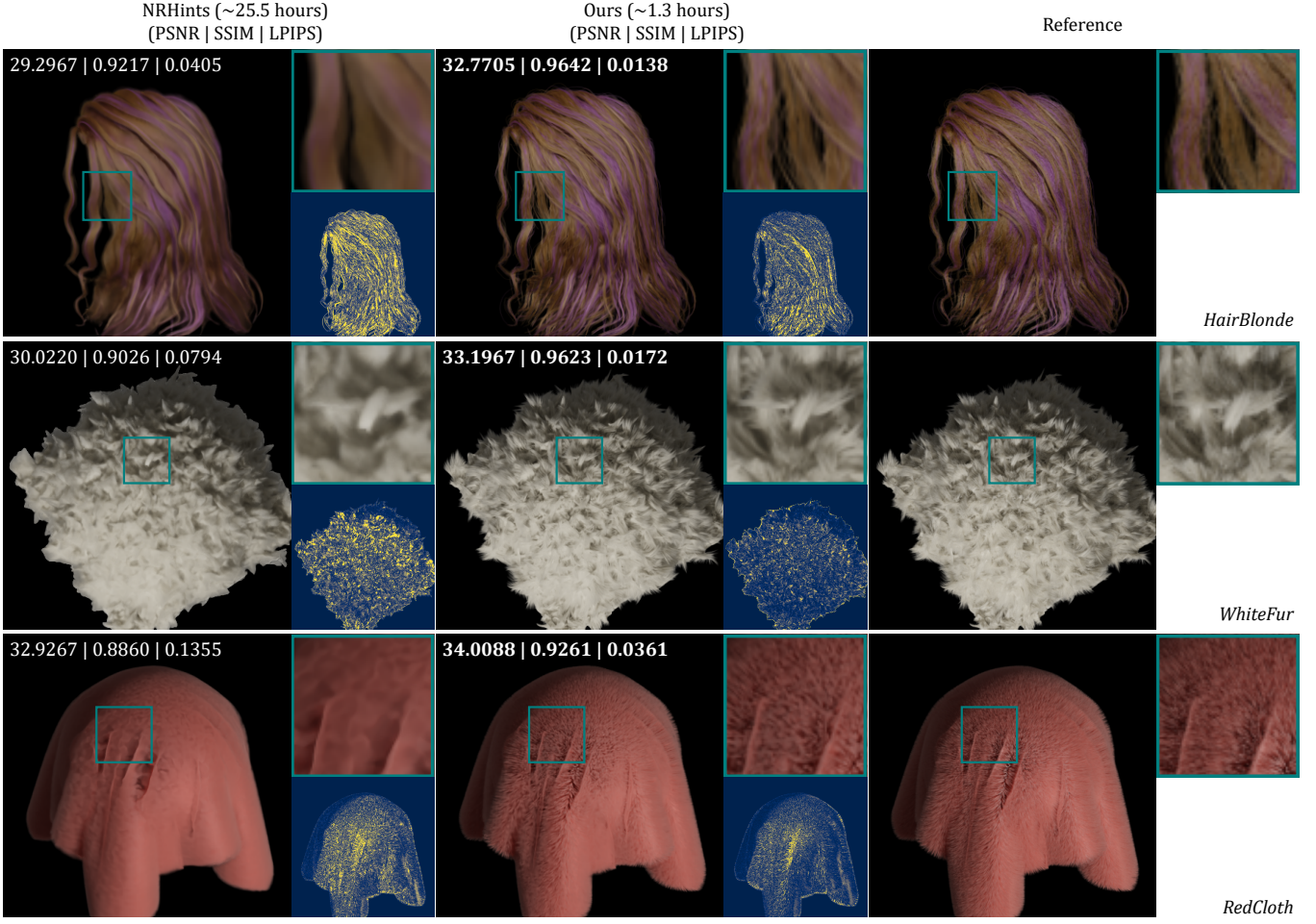


Fig. 7. Comparison between NRHINTs [Zeng et al. 2023] and our method on synthetic fluffy objects under point lighting. We provide PSNR, SSIM [Wang et al. 2004] and LPIPS [Zhang et al. 2018] for comparison. Our model can produce sharp details and plausible shadows with clear shapes while avoiding the over-smoothing issue for ill-defined shapes like hair and fur.

## 5.2 Ablation study

*Effect of depth refinement network.* In Fig. 9, we show the significance of the depth refinement network. With the refined depth, the renderer can more accurately locate the shading points and generate more reasonable shadow cues. With depth refinement, the shadow cue matches the reference better and can provide more powerful assistance to the final color.

*Ablation for all components.* In Fig. 10, we show the ablation of our model. We gradually remove the depth refinement MLP, the shadow-aware conditioning, and the second stage deferred shading optimization. The quality gap indicates the effectiveness and necessity of all the components of RNG.

## 5.3 Discussion and Limitations

*Precision of our representation.* RNG can relight various types of objects, including surface-based and fluffy ones. However, our model shows less accuracy in some scenes than NRHINTs [2023]. The main

reason is that NRHINTs uses SDF as a powerful prior, which is fairly slow and incompatible with fluffy objects. In contrast, we do not assume such surface constraints, being faster and more flexible for a wide range of object types.

*Shadow cue quality.* We deploy the shadow-aware conditioning to help the network predict the shadow appearance, leading to better-characterized shadows. However, the quality of shadows is still limited by the quality of shadow cues, which relies on a high-quality geometry reconstruction. On the one hand, the choice not to use ray marching limits the precision of our shadow cue. On the other hand, a perfect geometry reconstruction for fluffy objects is yet impossible. We suffer from the disadvantage in the geometry quality of 3DGS, like most of GS-based approaches.

*Complex material effects.* RNG can handle objects with both hard surfaces and ill-defined shapes. However, there are also many different kinds of complex materials in the real world, such as highly specular reflective surfaces and semi-transparent volumes. Since

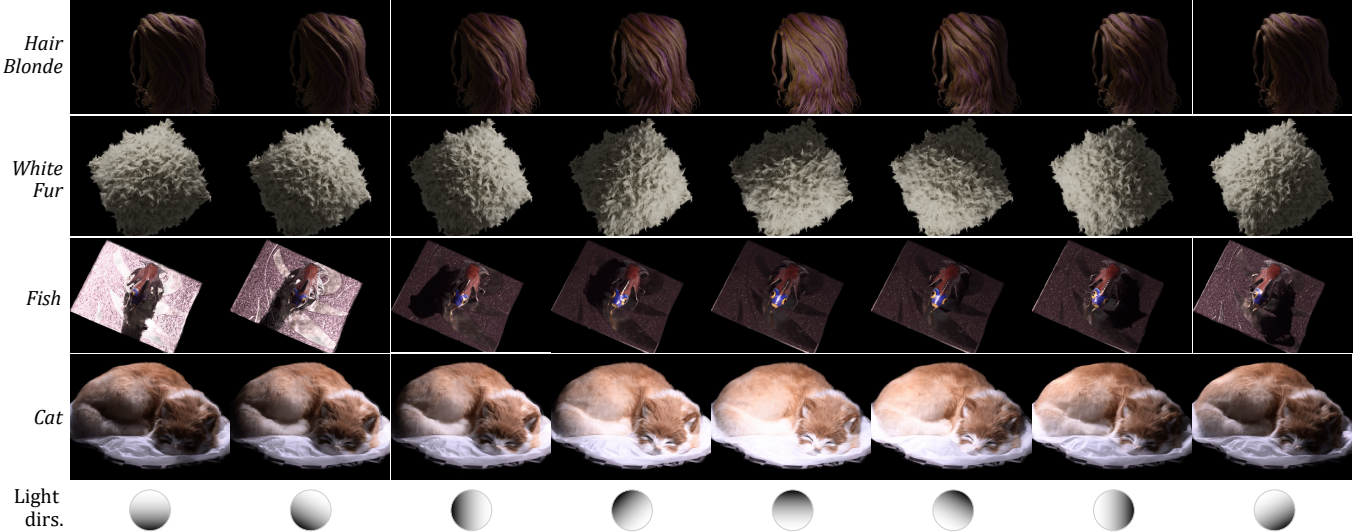


Fig. 8. The relighting results of Rnc. Each column shows a different light direction. Our model can render scenes in novel views and lights with realistic appearance with high-quality details, and can properly model the self-shadowing effects.

Table 1. Comparison of various scenes between NRHints [Zeng et al. 2023] and our method. We provide PSNR, SSIM [Wang et al. 2004] and LPIPS [Zhang et al. 2018] for comparison, and the prevailing results are marked as bold. Overall, we have lower LPIPS and close PSNR/SSIM values with significantly accelerated performance.

Scene	NRHints			Ours		
	(PSNR↑   SSIM↑   LPIPS↓)	(PSNR↑   SSIM↑   LPIPS↓)	(PSNR↑   SSIM↑   LPIPS↓)	(PSNR↑   SSIM↑   LPIPS↓)	(PSNR↑   SSIM↑   LPIPS↓)	(PSNR↑   SSIM↑   LPIPS↓)
Cat	<b>29.4956</b>   0.8803   0.1292	28.3869   <b>0.8883</b>   <b>0.0847</b>				
CatSmall	<b>35.4199</b>   <b>0.9740</b>   0.0477	34.4265   0.9688   <b>0.0382</b>				
CupFabric	37.8410   0.9824   0.0362	<b>38.8823</b>   <b>0.9863</b>   <b>0.0164</b>				
Fish	30.5272   0.9029   0.1135	<b>31.0113</b>   <b>0.9195</b>   <b>0.0561</b>				
FurScene	<b>32.3694</b>   <b>0.9441</b>   0.0615	29.8025   0.9369   <b>0.0501</b>				
Pikachu	<b>32.8470</b>   0.9637   0.0440	31.2147   <b>0.9665</b>   <b>0.0268</b>				
Pixiu	<b>32.1337</b>   <b>0.9375</b>   0.0734	29.8791   0.9044   <b>0.0684</b>				
FurBall	<b>31.8888</b>   <b>0.9340</b>   0.0524	27.6239   0.9239   <b>0.0441</b>				
Hotdog	<b>33.8954</b>   <b>0.9728</b>   <b>0.0227</b>	30.2335   0.9602   0.0332				
Lego	<b>29.5974</b>   <b>0.9559</b>   <b>0.0300</b>	26.6257   0.9226   0.0514				
HairBlonde	32.4588   0.9497   0.0388	<b>34.8082</b>   <b>0.9733</b>   <b>0.0146</b>				
WhiteFur	30.1356   0.9278   0.0605	<b>33.7007</b>   <b>0.9700</b>   <b>0.0140</b>				
RedCloth	34.0962   0.9186   0.1002	<b>35.2186</b>   <b>0.9489</b>   <b>0.0282</b>				
<i>Average</i>	<b>32.0896</b>   0.9384   0.0623	31.2336   <b>0.9412</b>   <b>0.0403</b>				

our model partially relies on the reconstruction capacity of 3DGS, it is potentially problematic when there are reflective or transparent regions in the scene. For such cases, maybe some assumptions should be added to better capture the object's geometry.

## 6 CONCLUSION AND FUTURE WORK

In this paper, we propose Rnc, a novel relightable asset with neural Gaussians. By introducing the relightable radiance representation,

we enable the relighting for both fluffy objects and surface-like scenes without any assumptions in the shading model and geometry types. In order to achieve this, we propose a neural implicit representation for the radiance at each Gaussian point, a shadow-aware conditioning with a depth refinement MLP for better shadow quality, as well as a hybrid forward-deferred optimization strategy. We achieve high-fidelity rendering and relighting under various lighting directions with a significantly improved training (within 1.5 hours) and rendering (60 fps) performance, compared to previous work.

There are still many potential future research directions. For example, involving some extensive light transport and complex surface scattering effects will be interesting and meaningful. Besides, trying to loosen the light conditions and support more flexible capturing setups is also challenging important. Another potential work is to explore more accurate depth estimation approaches for Gaussian point clouds since an accurate definition and solution for depths in Gaussian splatting can further improve the relighting quality and will definitely boost the down-stream research.

## REFERENCES

Jonathan T Barron, Ben Mildenhall, Matthew Tancik, Peter Hedman, Ricardo Martin-Brualla, and Pratul P Srinivasan. 2021. Mip-nerf: A multiscale representation for anti-aliasing neural radiance fields. In *Proceedings of the IEEE/CVF international conference on computer vision*. 5855–5864.

Jonathan T Barron, Ben Mildenhall, Dor Verbin, Pratul P Srinivasan, and Peter Hedman. 2022. Mip-nerf 360: Unbounded anti-aliased neural radiance fields. In *Proceedings of the IEEE/CVF conference on computer vision and pattern recognition*. 5470–5479.

Mojtaba Bemana, Karol Myszkowski, Hans-Peter Seidel, and Tobias Ritschel. 2020. X-fields: Implicit neural view-, light-and time-image interpolation. *ACM Transactions on Graphics (TOG)* 39, 6 (2020), 1–15.

Mark Boss, Raphael Braun, Varun Jampani, Jonathan T Barron, Ce Liu, and Hendrik Lenzsch. 2021a. Nerd: Neural reflectance decomposition from image collections. In *Proceedings of the IEEE/CVF International Conference on Computer Vision*. 12684–12694.

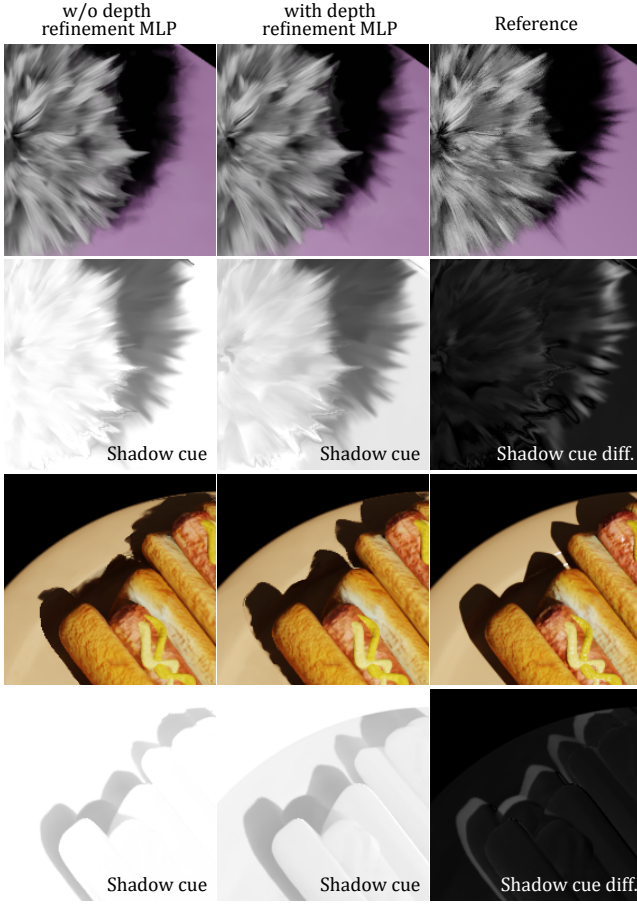


Fig. 9. The comparison of results with/without depth refinement MLP  $\Phi$  and the visualizations of corresponding shadow cues. With the depth refinement, the shadow mapping gives more reasonable and matched shadow cues, thus helping the network to better condition the appearance on the shadow information.

Mark Boss, Varun Jampani, Raphael Braun, Ce Liu, Jonathan Barron, and Hendrik Lensch. 2021b. Neural-pil: Neural pre-integrated lighting for reflectance decomposition. *Advances in Neural Information Processing Systems* 34 (2021), 10691–10704.

Brent Burley and Walt Disney Animation Studios. 2012. Physically-based shading at disney. In *AcM Siggraph*, Vol. 2012, vol. 2012, 1–7.

Anpei Chen, Zexiang Xu, Andreas Geiger, Jingyi Yu, and Hao Su. 2022. Tensorf: Tensorial radiance fields. In *European conference on computer vision*. Springer, 333–350.

Hanlin Chen, Chen Li, and Gim Hee Lee. 2023. Neusg: Neural implicit surface reconstruction with 3d gaussian splatting guidance. *arXiv preprint arXiv:2312.00846* (2023).

Pinxuan Dai, Jiamin Xu, Wenxiang Xie, Xinguo Liu, Huamin Wang, and Weiwei Xu. 2024. High-quality surface reconstruction using gaussian surfels. In *ACM SIGGRAPH 2024 Conference Papers*. 1–11.

Sara Fridovich-Keil, Alex Yu, Matthew Tancik, Qinzhong Chen, Benjamin Recht, and Angjoo Kanazawa. 2022. Plenoxels: Radiance fields without neural networks. In *Proceedings of the IEEE/CVF conference on computer vision and pattern recognition*. 5501–5510.

Duan Gao, Guojun Chen, Yue Dong, Pieter Peers, Kun Xu, and Xin Tong. 2020. Deferred neural lighting: free-viewpoint relighting from unstructured photographs. *ACM Transactions on Graphics (TOG)* 39, 6 (2020), 1–15.

Jian Gao, Chun Gu, Youtian Lin, Hao Zhu, Xun Cao, Li Zhang, and Yao Yao. 2023. Relightable 3d gaussian: Real-time point cloud relighting with brdf decomposition and ray tracing. *arXiv preprint arXiv:2311.16043* (2023).

Antoine Guédon and Vincent Lepetit. 2024. Sugar: Surface-aligned gaussian splatting for efficient 3d mesh reconstruction and high-quality mesh rendering. In *Proceedings of the IEEE/CVF Conference on Computer Vision and Pattern Recognition*. 5354–5363.

Eric Heitz, Jonathan Dupuy, Cyril Crassin, and Carsten Dachsbacher. 2015. The SGX microflake distribution. *ACM Transactions on Graphics (TOG)* 34, 4 (2015), 1–11.

Binbin Huang, Zehao Yu, Anpei Chen, Andreas Geiger, and Shenghua Gao. 2024. 2d gaussian splatting for geometrically accurate radiance fields. In *ACM SIGGRAPH 2024 Conference Papers*. 1–11.

Yingwenqi Jiang, Jiadong Tu, Yuan Liu, Xifeng Gao, Xiaoxiao Long, Wenping Wang, and Yuexin Ma. 2024. Gaussianshader: 3d gaussian splatting with shading functions for reflective surfaces. In *Proceedings of the IEEE/CVF Conference on Computer Vision and Pattern Recognition*. 5322–5332.

Haian Jin, Isabeli Liu, Peijia Xu, Xiaoshuai Zhang, Songfang Han, Sai Bi, Xiaowei Zhou, Zexiang Xu, and Hao Su. 2023. Tensori: Tensorial inverse rendering. In *Proceedings of the IEEE/CVF Conference on Computer Vision and Pattern Recognition*. 165–174.

James T Kajiya. 1986. The rendering equation. In *Proceedings of the 13th annual conference on Computer graphics and interactive techniques*. 143–150.

Bernhard Kerbl, Georgios Kopanas, Thomas Leimkühler, and George Drettakis. 2023. 3D Gaussian Splatting for Real-Time Radiance Field Rendering. *ACM Trans. Graph.* 42, 4 (2023), 139–1.

Diederik P Kingma and Jimmy Ba. 2014. Adam: A method for stochastic optimization. (2014). *arXiv:2312.05133*

Jia Li, Lu Wang, Lei Zhang, and Beibei Wang. 2024. Tensosdf: Roughness-aware tensorial representation for robust geometry and material reconstruction. *ACM Transactions on Graphics (TOG)* 43, 4 (2024), 1–13.

Zhihao Liang, Qi Zhang, Ying Feng, Ying Shan, and Kui Jia. 2024. Gs-ir: 3d gaussian splatting for inverse rendering. In *Proceedings of the IEEE/CVF Conference on Computer Vision and Pattern Recognition*. 21644–21653.

Yuan Liu, Peng Wang, Cheng Lin, Xiaoxiao Long, Jiepeng Wang, Lingjie Liu, Taku Komura, and Wenping Wang. 2023. Nero: Neural geometry and brdf reconstruction of reflective objects from multiview images. *ACM Transactions on Graphics (TOG)* 42, 4 (2023), 1–22.

Ben Mildenhall, Pratul P Srinivasan, Matthew Tancik, Jonathan T Barron, Ravi Ramamoorthi, and Ren Ng. 2021. Nerf: Representing scenes as neural radiance fields for view synthesis. *Commun. ACM* 65, 1 (2021), 99–106.

Thomas Müller, Alex Evans, Christoph Schied, and Alexander Keller. 2022. Instant neural graphics primitives with a multiresolution hash encoding. *ACM transactions on graphics (TOG)* 41, 4 (2022), 1–15.

Krishna Mullia, Fujun Luan, Xin Sun, and Miloš Hašan. 2024. RNA: Relightable Neural Assets. *ACM Transactions on Graphics* (2024).

Adam Paszke, Sam Gross, Francisco Massa, Adam Lerer, James Bradbury, Gregory Chanan, Trevor Killeen, Zeming Lin, Natalia Gimelshein, Luca Antiga, et al. 2019. Pytorch: An imperative style, high-performance deep learning library. *Advances in neural information processing systems* 32 (2019).

Peiran Ren, Yue Dong, Stephen Lin, Xin Tong, and Baining Guo. 2015. Image based relighting using neural networks. *ACM Transactions on Graphics (ToG)* 34, 4 (2015), 1–12.

Radu Alexandru Rosu and Sven Behnke. 2023. Permutosdf: Fast multi-view reconstruction with implicit surfaces using permutohedral lattices. In *Proceedings of the IEEE/CVF Conference on Computer Vision and Pattern Recognition*. 8466–8475.

Yahao Shi, Yanmin Wu, Chenming Wu, Xing Liu, Chen Zhao, Haocheng Feng, Jingtuo Liu, Liangjun Zhang, Jian Zhang, Bin Zhou, et al. 2023. Gir: 3d gaussian inverse rendering for relightable scene factorization. *arXiv preprint arXiv:2312.05133* (2023).

Dor Verbin, Peter Hedman, Ben Mildenhall, Todd Zickler, Jonathan T Barron, and Pratul P Srinivasan. 2022. Ref-nerf: Structured view-dependent appearance for neural radiance fields. In *2022 IEEE/CVF Conference on Computer Vision and Pattern Recognition (CVPR)*. IEEE, 5481–5490.

Peng Wang, Lingjie Liu, Yuan Liu, Christian Theobalt, Taku Komura, and Wenping Wang. 2021. Neus: Learning neural implicit surfaces by volume rendering for multi-view reconstruction. *arXiv preprint arXiv:2106.10689* (2021).

Zhou Wang, Alan C Bovik, Hamid R Sheikh, and Eero P Simoncelli. 2004. Image quality assessment: from error visibility to structural similarity. *IEEE TIP* (2004).

Zixiong Wang, Yunxia Zhang, Rui Xu, Fan Zhang, Peng-Shuai Wang, Shuangmin Chen, Shiqing Xin, Wenping Wang, and Changhe Tu. 2023. Neural-Singular-Hessian: Implicit Neural Representation of Unoriented Point Clouds by Enforcing Singular Hessian. *ACM Transactions on Graphics (TOG)* 42, 6 (2023), 1–14.

Zexiang Xu, Kalyan Sunkavalli, Sunil Hadap, and Ravi Ramamoorthi. 2018. Deep image-based relighting from optimal sparse samples. *ACM Transactions on Graphics (ToG)* 37, 4 (2018), 1–13.

Ziyi Yang, Yanzhen Chen, Xinyu Gao, Yazhen Yuan, Yu Wu, Xiaowei Zhou, and Xiaogang Jin. 2023. Sire-ir: Inverse rendering for brdf reconstruction with shadow and illumination removal in high-illuminance scenes. *arXiv preprint arXiv:2310.13030* (2023).

Chong Zeng, Guojun Chen, Yue Dong, Pieter Peers, Hongzhi Wu, and Xin Tong. 2023. Relighting neural radiance fields with shadow and highlight hints. In *ACM SIGGRAPH 2023 Conference Proceedings*. 1–11.

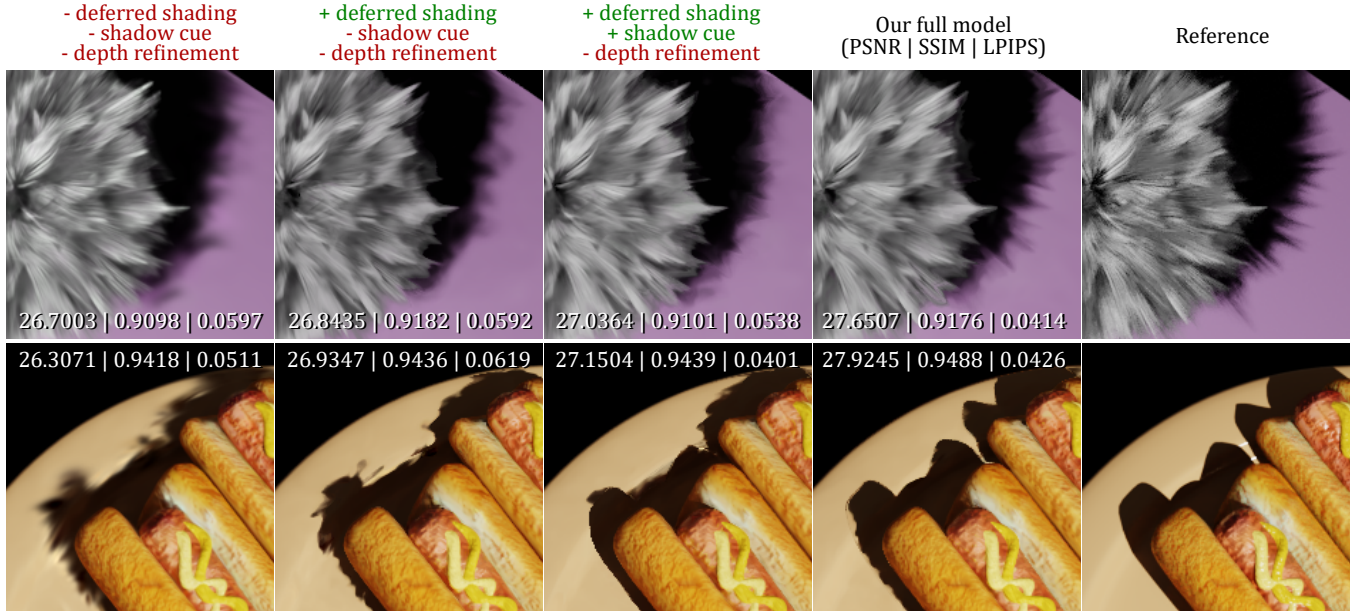


Fig. 10. The ablation study of components in RNC. We prove the importance and necessity of the second stage deferred shading optimization, the shadow cue, and the depth refinement network. We gradually remove them from our full model and show the quality gap between them. Although it is not very challenging for the network to represent the object’s appearance, the quality of shadows is significantly improved by adding these components to our model.

Jingyang Zhang, Yao Yao, Shiwei Li, Jingbo Liu, Tian Fang, David McKinnon, Yanghai Tsin, and Long Quan. 2023b. Neif++: Inter-reflectable light fields for geometry and material estimation. In *Proceedings of the IEEE/CVF International Conference on Computer Vision*. 3601–3610.

Kai Zhang, Fujun Luan, Qianqian Wang, Kavita Bala, and Noah Snavely. 2021a. Physg: Inverse rendering with spherical gaussians for physics-based material editing and relighting. In *Proceedings of the IEEE/CVF Conference on Computer Vision and Pattern Recognition*. 5453–5462.

Richard Zhang, Phillip Isola, Alexei A Efros, Eli Shechtman, and Oliver Wang. 2018. The unreasonable effectiveness of deep features as a perceptual metric. In *CVPR*.

Xiuming Zhang, Pratul P Srinivasan, Boyang Deng, Paul Debevec, William T Freeman, and Jonathan T Barron. 2021b. Nerfactor: Neural factorization of shape and reflectance under an unknown illumination. *ACM Transactions on Graphics (ToG)* 40, 6 (2021), 1–18.

Youjia Zhang, Teng Xu, Junqing Yu, Yuteng Ye, Yanqing Jing, Junle Wang, Jingyi Yu, and Wei Yang. 2023a. Nemf: Inverse volume rendering with neural microflake field. In *Proceedings of the IEEE/CVF International Conference on Computer Vision*. 22919–22929.